The Microclimates of the Arctic Tundra

GUNTER WELLER AND BJORN HOLMGREN

Geophysical Institute, University of Alaska, Fairbanks 99701

(Manuscript received 13 November 1973, in revised form 24 July 1974)

ABSTRACT

The microclimates of the arctic tundra at Barrow, Alaska, are described for the near-surface terrestrial layers in which most biological activities take place. Temperature profiles are constructed from detailed measurements in the air, vegetation and soil, from 16 m above to 6 m below the tundra surface. Wind and radiation measurements supplement these data. Considering the tundra as a two-dimensional heat exchange surface, daily components of the heat balance are computed and summarized for a number of periods throughout the year, which are characterized by changes of the physical nature of the tundra surface such as appearance and disappearance of snow, meltwater and precipitation, and growth and decay of vegetation. Through changes in surface terrain parameters such as albedo and roughness length, and availability of water for phase changes, the thermal and moisture regimes of the near-surface layer change markedly during these periods as reflected by the heat balance.

1. Introduction

Climate and microclimate are dynamic forces which shape the environment to a considerable degree. In the Arctic, the most dynamic environmental events take place during the brief spring and autumn. Specifically the transitions from snow to snow-free surface and vice-versa cause startling differences in the microclimate regimes.

To investigate these differences, the microclimates of the arctic tundra at Barrow, Alaska, were the subject of intensive studies during 1971 and 1972. These investigations were carried out within the framework of the Tundra Biome of the International Biological Program. The present paper summarizes results available to date. To achieve a quantitative understanding of the microclimate, energy balance considerations were applied to the data, and the causes and effects of the various balance components such as radiation, convection, etc., were analyzed. Heat sources and sinks were thus identified numerically and their seasonal variation and effect on the climate determined. This partitioning of the available energy, and examination of the physical factors underlying the partitioning, allow extrapolation to hypothetical environments and facilitate modeling efforts. The data were collected on the flat tundra, approximately 3 km inland from the coast, using an array of standard micrometeorological equipment and a data logger capable of recording the data on punched paper tape. The equipment used included a CSIRO net radiometer and Eppley pyranometers, "Climet" 3-cup wind speed sensors and wind direction sensors, and "Climet" ventilated and standard unventilated thermocouples for measuring air temperatures and all other temperatures, respectively, by comparing their output with that of a 0C "Kaye" reference cell. The wind and temperature sensors were mounted on a tower at 0.5, 1, 2, 4, 8 and 16 m; temperature sensors in the vegetation and snow were at 5-cm vertical intervals and in the soil at 2-cm intervals down to 10 cm, then at 10-cm intervals down to 1 m, with additional sensors at 2, 4 and 6 m. The considerable frosting problems on the lower instrumentation, particularly the anemometers, in winter, were successfully overcome by using heat lamps radiating on each anemometer. Special equipment, where used, is described in the appropriate sections of this paper.

2. Radiation

As elsewhere in the global terrestrial system, radiation is the dominant term in the arctic energy balance. The two most important environmental features influencing the radiation regime of the arctic tundra are the seasonal snow cover present during nine months of each year and the prevailing low stratus cloud decks during summer. The snow cover, through its high albedo of over 80%, reflects most of the incident solar energy back into space. This is particularly important during spring when relatively high solar elevation angles and long duration of daylight (Table 1) ensure a large solar energy flux toward the surface. The tundra is snow-free from mid-June to mid-September. Fig. 1 shows variations in albedo of the tundra. Dry snow, present during most of the

TABLE 1. Astronomical factors affecting solar radiation fluxes at the terrestrial surface.

	Jan.	Feb.	Mar.	Apr.	May	Jun.	Jul.	Aug.	Sep.	Oct.	Nov.	Dec.
Noon solar elevations* (deg)	−2.4	6.1	17.1	28.9	37.8	42.1	40.0	32.3	21.3	9.8	−0.1	−4.6
Possible duration of sunshine* (hr)	0	6.8	11.5	16.5	24	24	24	19	13.5	8.8	0	0

* On the 15th day of each month.

year, has an average albedo value of approximately 85%. Generally somewhat lower values are measured for a clear sky and somewhat higher values for an overcast sky. It may be seen that the albedo curve during the snow-melt period is convex to the right, i.e., the decrease of the albedo becomes increasingly rapid. This indicates that the decay of the snow pack accelerates as the snow cover becomes thinner and bare patches appear (O'Neill and Gray, 1972). The albedo drops steadily during melting to a low value of 15% after complete snow melt, when the tundra is covered with water puddles. Dry tundra has mean albedo values of ~20%; whenever rain or snow melt produce extensive areas of water the albedo is reduced to 15% again, as shown in Fig. 1.

Spot measurements of albedos over a variety of different tundra surfaces, both natural and manipulated, were reported earlier (Brown and West, 1970) and are summarized in Table 2.

Low stratus clouds are present almost continually over Barrow throughout the summer. When they consist of a single layer only, their mean cloud top albedo is 55%, while the more frequent multi-layered clouds have mean albedos of 65% as measured both times over snow-free tundra (Jayaweera and Weller, 1972). Apart from modifying the infrared radiation fluxes and the near-surface thermal regime, they are thus also able to reflect large amounts of incident solar energy back to space. The following simple matrix (Table 3) shows the effects of cloud and tundra surface albedos on the amount of solar radiation absorbed by the surface, and hence available for utilization as a source in the energy balance. Global radiation (incoming direct solar and diffuse sky radiation on a horizontal surface) is taken as 100%. The clouds are assumed to absorb 5% of the incoming radiation, and multiple scattering effects between cloud and surface (which raise the albedo slightly) are accounted for by a simplified scheme (cf. Liljeqvist, 1956):

$$G_{10}=G_0(1-W)\frac{1-A_c}{1-AA_c},$$

where:

G_{10} insolation at surface with 10/10 cloud cover
G_0 insolation at surface with clear skies
A surface albedo
A_c cloud albedo
W fractional absorption by cloud.

Realistic combinations of wet tundra (15% albedo), dry tundra (20%), snow-covered tundra (80% and 87% for clear and overcast skies, respectively), single-layer stratus clouds (55%), multi-layered stratus clouds (65%) and clear skies (0%) are enclosed in parentheses. The amounts of available solar energy at the tundra surface are seen to vary from 10 to 85% for

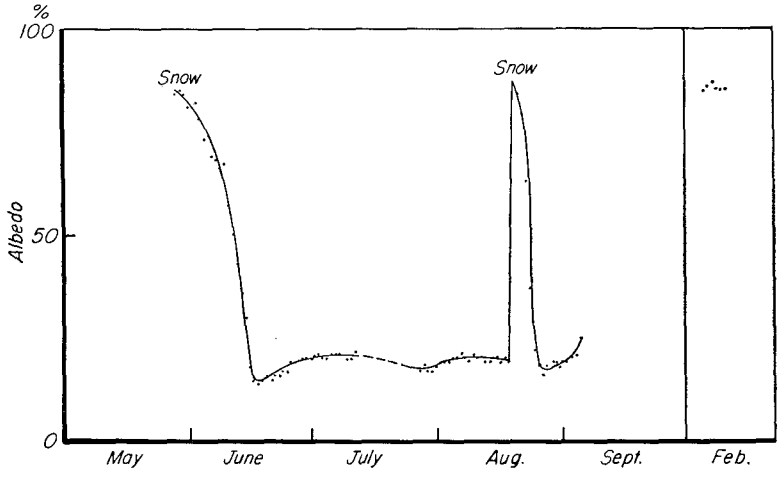

FIG. 1. The albedo of the tundra surface.

TABLE 2. Albedos of natural and manipulated tundra surfaces.

Surface type	Range of measurements	Representative value
Dry ground	23–26	24
Wet ground	11–20	16
Water-filled vehicle tracks	10–11	10
Vehicle tracks, no water	13–21	16
Oil spills on dry ground	17–22	20

these combinations. Both cloud and surface albedo thus exert strong control over the amount of solar energy available as a heat source at the tundra surface.

Table 4 shows measured values of the global radiation incident at the tundra surface, and the all-wave net radiation for mean cloud conditions for the three summer months of 1971. The data are compared with those reported by Maykut and Church (1973) for the period 1962–66 at Barrow.

Radiation penetrates both the snow and the tundra vegetation. Extinction of light in both media was measured on numerous occasions and in different locations with selenium photocells (response peak 0.6 μm, bandwidth 0.3–0.7 μm). The mean extinction coefficient for the snow at Barrow was 0.10 cm^{-1}, reducing the transmitted radiation at the snow surface from 100% to 37% at 10 cm depth, 13% at 20 cm depth and 1% at the bottom of the snow pack at 45 cm depth. In the tundra vegetation, the exponential extinction law does not apply since the medium is not homogeneous, with leaf area indices varying throughout the vegetation. At 12 cm above the soil surface, approximately the maximum height of the vegetation, incoming radiation is 100%, at 8 cm 80%, at 5 cm 60%, at 2 cm 35%, and at the surface 15%. This gives a mean equivalent extinction coefficient of 0.16 cm^{-1}. Appreciable reductions in light intensities thus occur in both snow and vegetation.

3. Heat flux in soil and snow

Heat transfer in the soil takes place mainly by molecular conduction, although freezing and thawing of the soil in the upper 40 cm also create latent heat sources and sinks, and convection of water in the soil matrix may occur in summer, with associated heat transfer. No quantitative information is available on the latter effect and it has been neglected in the present considerations. The soil at Barrow consists of two layers: a top organic layer ~5–10 cm thick and an inorganic soil layer underneath. Thermal properties of these layers were taken from Brown and West (1970, p. 24). The thermal conductivity of the inorganic layer is eight times higher than that of the organic layer. This results in temperature gradients being steepest in the top organic layer. The thermal regimes of the tundra soils at Barrow have been examined and modeled by Nakano and Brown (1972).

Thermal characteristics of the snow as a function of densities and temperatures were taken from the paper by Weller and Schwerdtfeger (1970). Convective heat and mass transfer within the dry snow cover, which is known to exist in the seasonal snow cover of Alaska (Trabant *et al.*, 1969) was neglected. Since the heat flux in soil and snow is very small compared with other components of the heat balance at the terrestrial surface, as will be shown in the following, this neglect is not serious. During the snow-melt period the temperature gradient within the snow pack becomes essentially isothermal. By refreezing of meltwater at the soil-snow interface, a relatively efficient energy transfer may then be maintained across the snow pack. Daily heat fluxes in the subsurface media were computed based on changes in heat content, which in turn were computed from subsurface temperature profiles.

TABLE 3. Cloud and surface albedo matrix, determining amount of solar energy absorbed at the surface.*

Surface type	Surface albedo	Cloud albedo: Single layer (55)	Cloud albedo: Multiple layer (65)	Cloud albedo: Clear sky
Tundra, wet	(15)	39	30	85
Tundra, dry	(20)	38	29	80
Snow, clear sky	(80)	—	—	20
Snow, overcast	(87)	12	10	—

* Expressed in percent of incoming radiation for days with clear skies, rounded off to closest whole number. Albedo values are within parentheses.

TABLE 4. Global and net radiation for mean cloud conditions at Barrow (cal cm^{-2} day^{-1}).

	June	July	August	
Global radiation	662	461	274	Weller and Holmgren, 1971
	568	421	246	Maykut and Church, 1962–66
Net radiation	274	259	130	Weller and Holmgren, 1971
	217	263	158	Maykut and Church, 1962–66

4. Eddy sensible heat flux

Heat is transferred toward and away from the tundra surface by eddy turbulent processes. Detailed observations of wind and temperature profiles were made to determine the nature of the heat transfer by these processes. Average temperature profiles above the vegetation canopy indicated lapse rates close to adiabatic during summer but showed steep inversions and stable stratifications during winter. An index of the atmospheric stability is the Richardson number,

the ratio of buoyancy to inertia forces:

$$\mathrm{Ri}=\frac{g\Delta z\Delta\theta}{T_m(\Delta V)^2}, \tag{1}$$

where g is the acceleration of gravity, Δz the height difference between two pairs of sensors used to determine potential temperature differences ($\Delta\theta$) and wind speed differences (ΔV), and T_m the mean temperature of the layer between the sensors. Daily Richardson numbers, as based on half-hourly values and computed for the layer between 2–8 m, lay in the following ranges:

Period	Mean	Range
Summer (29 May–1 Sept.)	−0.052	0.012 to −0.163
Winter (5–10 Feb.)	0.702	0.606 to 0.788

The strongest inversion observed during the winter period was approximately 20C between the snow surface and the top of the tower at 16 m. Mean inversion strength over the same height was 13.6C. During summer, at 16 m, temperatures were in the mean 0.8C cooler than at 0.5 m. An additional mean temperature increase of 2.5C occurred between 0.5 m and the soil surface, mostly within the vegetation canopy.

Wind profiles over the summer tundra showed approximately logarithmic increases with height, as expected for the near-neutrally stratified air, according to

$$u=\frac{u_*}{k}\ln\frac{z}{z_0}, \tag{2}$$

where u is the wind velocity at height z, k von Kármán's constant, and u_* the friction velocity. The roughness parameter z_0 is related to the height and spacing of the micro- and macro-roughness elements of the surface. In winter, when a smooth snow cover exists, z_0 is found to be 0.03 cm on the average. Immediately after snow melt, when water covers a large surface area, z_0 increases to 0.4 cm and when the tundra vegetation is fully developed during summer, z_0 has values between 2–4 cm.

The tundra vegetation modifies the logarithmic profile close to the ground. To express the wind profile above the vegetation canopy, an additional term, the zero-displacement parameter d is introduced:

$$u=\frac{u_*}{k}\ln\left(\frac{z-d}{z_0}\right). \tag{3}$$

By measuring winds close to the upper vegetation boundary using hot wire anemometers, the shape of the wind profile could be obtained and the term d could be computed. For typical tundra vegetation, consisting mainly of *Eriophorum angustifolium* and *Depontia fischeri*, $d\approx 5$ cm. For sparser vegetation (*Petasites frigidus* and *Arctograstic latifolia*) $d\approx 2$ cm. In considering transfer processes, such as heat, water and CO_2 close to the tundra surface, the zero displacement parameter enters as an important correction term. Wind profiles were also measured within the vegetation, both in undisturbed and in manipulated canopies. The complete wind profiles for these cases up to 2 m are shown in Fig. 2.

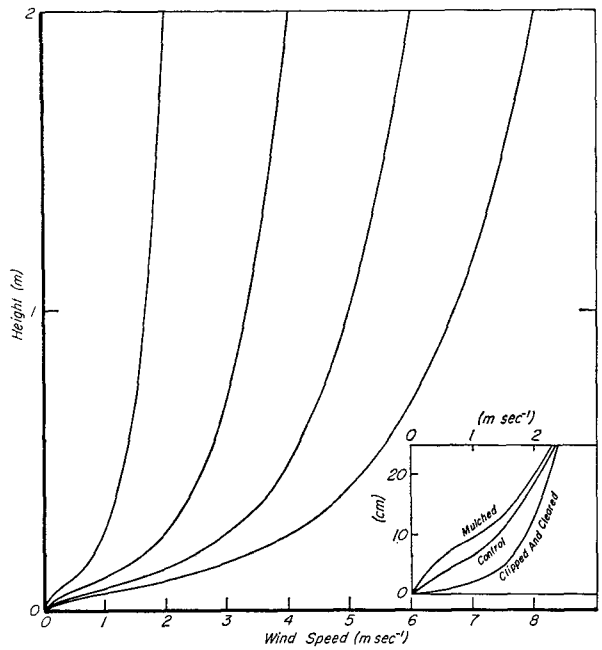

FIG. 2. Wind profiles above and within the vegetation canopy. The insert shows details of the profiles in and above modified canopies, normalized for a wind speed of 4.5 m sec^{-1} at 2 m height, the average summer wind speed in 1971.

Using a scheme developed by Lettau (1949), the eddy heat flux can be computed from

$$Q=\rho C_p A\frac{d\theta}{dz}, \tag{4}$$

where the exchange coefficient for diabatic conditions is

$$A=\frac{A_a}{(1+\mathrm{Ri})^2}, \tag{5}$$

and A_a, the exchange coefficient for adiabatic conditions, is

$$A_a=ku_*z. \tag{6}$$

In the above Q is the eddy heat flux, C_p the specific heat of air at constant pressure [0.24 cal gm^{-1} (°C)$^{-1}$], and $d\theta/dz$ the potential temperature gradient.

Eq. (5) should primarily be applicable for stability conditions not too far from neutral. For the present purpose, to discuss the main features of the tundra energy regime, it is judged that the above scheme might be applied for average daily wind and tem-

FIG. 3. Appearance of the water-saturated tundra during the last stages of snow melting. Note evaporation tank on left, water-filled old snow-machine track, and vehicle tracks made by compaction of snow. (Photo taken from top of micrometeorological tower.)

perature profiles in summer. Barrow is a rather windy place (Fig. 7), and near-neutral stability is encountered most of the time in summer.

5. Latent heat flux

Latent heat enters the energy balance considerations through snow melting and sublimation and water evaporation processes. Although dew point sensors were installed on the tower at Barrow to obtain atmospheric moisture profiles, these did not perform well and all data were discarded. Latent heat fluxes, therefore, had to be computed as remainder terms in the energy balance equation. However, these calculations were supported by direct measurements from evaporation pans during summer. Particularly after snow melt, the tundra is completely water-soaked, with a high percentage of the surface consisting of water puddles (see Fig. 3). Under these conditions, evaporation rates from Class A standard pans are probably quite representative for the tundra surface. The agreement is, in fact, quite good, not only for the period immediately following snow melt, but also through most of summer since the tundra remains mostly wet. This will be demonstrated in detail below.

6. Heat balance

From a synthesis of the individual heat balance components discussed above, the total balance can be obtained. The balance equation can be written

$$N+Q+S+E=0, \tag{8}$$

where N is the net radiation, Q the eddy sensible heat flux, S the heat flux in soil and snow, and E the latent heat flux.

The chosen sign convention is such that a heat flux toward the surface is termed positive (heat source) and a flux away from the surface negative (heat sink). Heat balances were computed for the periods shown in Table 5, each one characterizing a major change in the physical appearance of the tundra. These balances are computed from the mean of daily values of each period and are shown in Fig. 4.

The most dramatic changes in the energy balance take place when the snow melts in spring. This is demonstrated on a day-to-day basis in Fig. 5 as reported previously (Weller *et al.*, 1972). As the snow albedo decreases during melting, more solar energy is absorbed. The absorbed energy is increased by an order of magnitude with the complete disappearance

TABLE 5. Periods for which heat balances were computed marking different seasonal phases characterizing the tundra surface.

Period	Phase	Dates	Duration (days)	Average cloudiness (tenths)	Average deviation from temperature normals 1931–60 (°C)
1	pre-melting	29 May–3 June, 1971	6	10	+1.7
2	snow melting	4–13 June 1971	10	6	+1.6
3	post-melting	14–17 June 1971	4	7	+1.0
4	mid-summer	15–28 July 1971	14	8	+1.2
5	freeze-up	25 Aug.–1 Sep., 1971	8	10	−3.3
6	mid-winter	5–10 Feb. 1972	6	3	−5.0

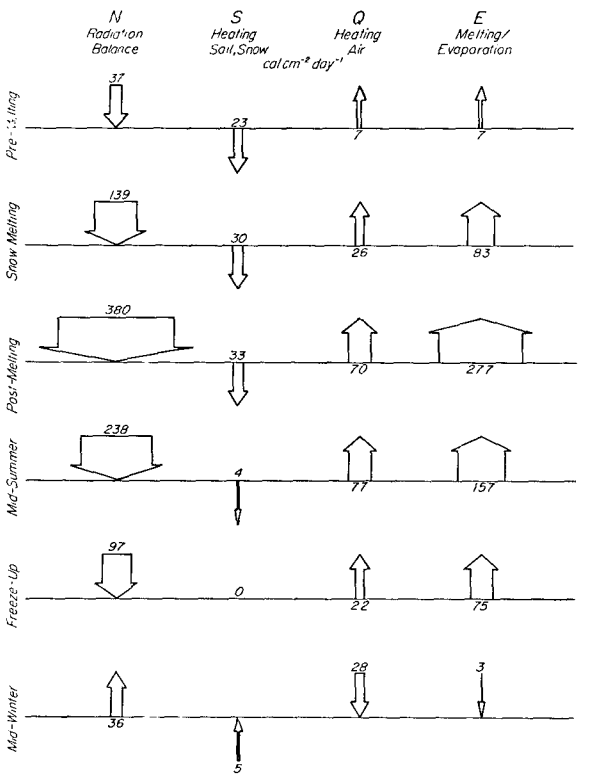

FIG. 4. Heat balances for six different characteristic periods. The width and direction of the arrows and numbers at the base of each arrow indicate energy flux directions and rates (cal cm^{-2} day^{-1}).

of the snow cover. This available energy is used to heat the soil (9%), heat the air (18%), and evaporate water off the tundra surface (73%). The evaporation reaches maximum rates up to 6 mm day^{-1} and mean values of 4.5 mm day^{-1}. Through the melting phase, within the span of 2–3 weeks, the net radiation has increased by a factor of 10 and the latent heat flux by a factor of 40.

During mid-summer the available solar energy is distributed as follows: heating of soil—2%, heating of air—32%, evaporation—66%, although now mean evaporation rates have dropped to 2.6 mm day^{-1}. By the time freezing of the tundra surface occurs in early September, radiation values have dropped appreciably and evaporation has been reduced further to ~1.1 mm day^{-1}. Soon thereafter snow covers the tundra again and the radiation balance becomes negative. This marks the second drastic seasonal change, eventually reversing the direction of flux of every one of the balance components.

For the winter heat balance, the method outlined above for computing the eddy heat flux could not be used, since the Richardson numbers were too high. In this case latent heat fluxes were computed from mass changes of carefully exposed pans, to obtain frost deposit rates by sublimation, and the eddy heat fluxes were deduced as remainder terms in the balance equation. The radiative losses during that period (100%) were compensated by eddy heat flux toward the snow surface (78%), soil heat flux (14%), and latent heat release (8%) when frost forms on the surface. These results could not be verified independently, unlike the summer balances. These values must therefore be taken to represent order of magnitude only. The winter phase characterizes the true nature of the arctic tundra as part of the polar heat sink.

7. The thermal regimes of the tundra

The energy balances show the amounts of heat available to warm air and soil. The heat input into the air increases by an order of magnitude from early spring to summer, while for the soil it decreases from a maximum of 33 to 4 cal cm^{-2} day^{-1}, and later to zero by the time freezing of the tundra occurs. During the snow-melt period, the average air temperature is 0.8C while the snow surface is close to 0C. At the same time there is a net flux of heat in the air, which might be explained by the rapid solar heating of the snow-free patches forming at the end of the melt

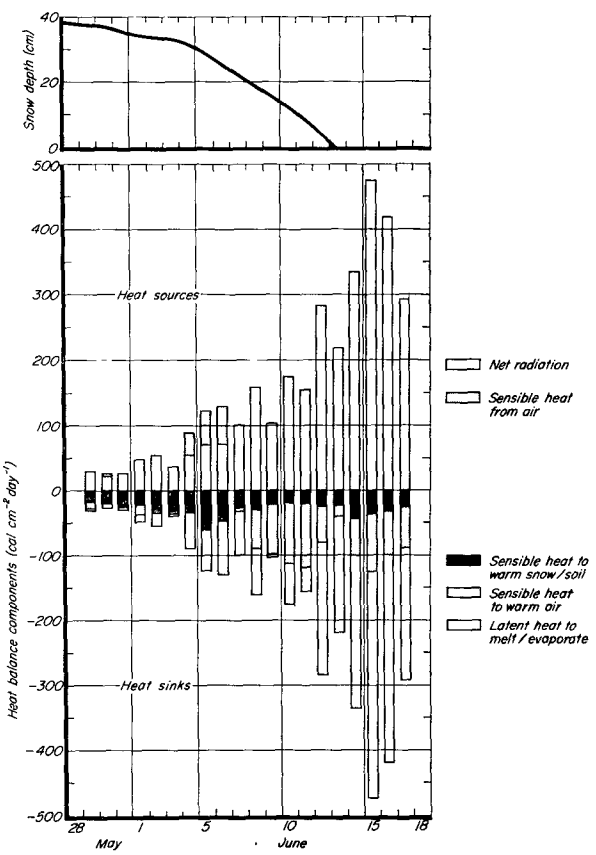

FIG. 5. Daily heat balances through the snow-melt period. The top diagram indicates the snow depths during this period.

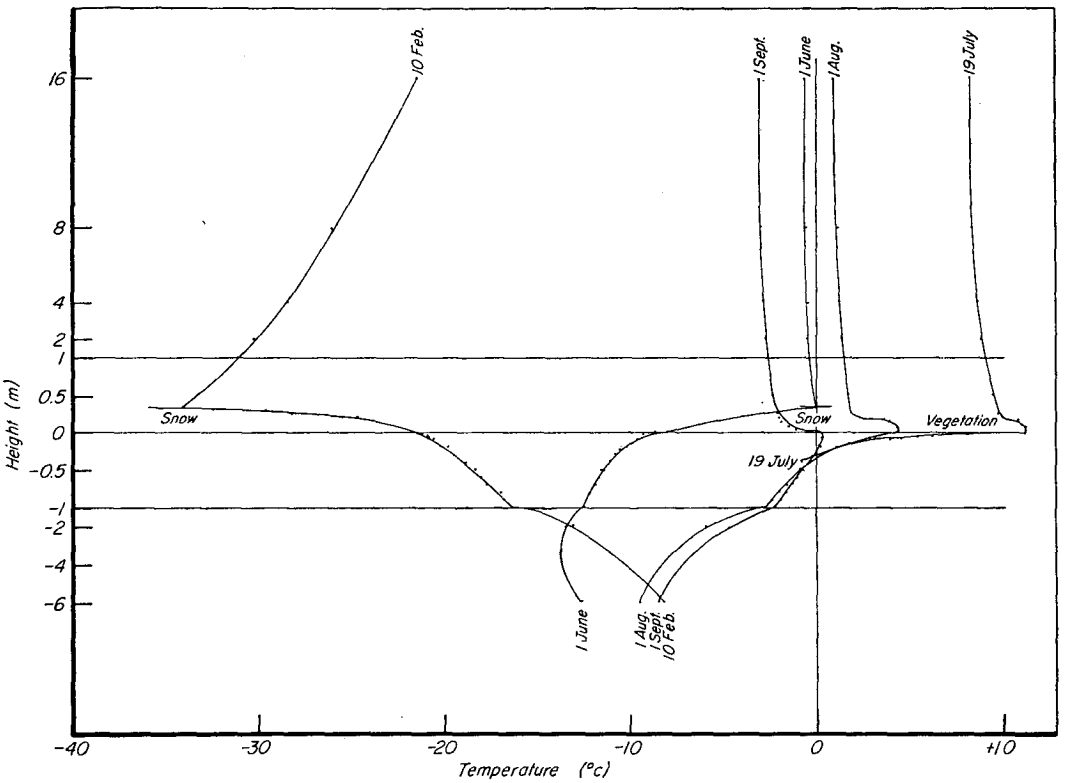

FIG. 6. Typical temperature gradients in air, snow, vegetation and soil. Note the effects of snow (10 February and 1 June) and vegetation (1 August and 19 July) on the soil surface temperature. The vertical height scale from +1 to −1 m is expanded.

period. The thermal regime is characterized by some typical temperature profiles in Fig. 6 in which measured temperature data from 16 m above to 6 m below the soil surface are presented. The effects of snow and vegetation on the temperature of the soil surface are clearly shown in the expanded section of the diagram from +1 to −1 m height. Moderate to strong inversions exist in the air in winter; the typical example of 10 February shows the 16 m temperature to be warmer by about 13C than the snow surface. On the other hand, lapse rate conditions in summer ensure that the highest temperatures occur at the surface. In winter the snow cover provides considerable thermal protection to the soil surface regime, which is 10–15C warmer than the snow surface. The reverse is true early in spring when the snow surface is 5–10C warmer than the soil surface. Temperatures within the vegetation canopy are seen to be 2–3C higher than in the air immediately above the canopy. Maximum thaw depth is seen to be ~40 cm.

8. The moisture regimes of the tundra

The application of results of the energy balance computations now allow a quantitative interpretation of the moisture regimes of the tundra, specifically evaporation rates. Fig. 4 gives the daily latent heat flux values for the six periods under consideration. When the air temperature is below zero, sublimation latent heats of 680 cal cm^{-1} are used to convert the latent heat flux to daily sublimation or deposition rates (periods 1, 5 and 6). Similarly, latent heats of evaporation of 600 cal gm^{-1} were used during the summer (periods 3 and 4). The snow melting period (period 2) presents some difficulty in interpretation, since latent heats for melting and evaporation cannot be separated easily. Assuming the snow cover with a depth of 33 cm and mean density of 0.28 gm cm^{-3} to melt in 10 days [slightly revised from previous estimates published (Weller *et al.*, 1972)], daily ablation rates of 9 mm of water equivalent are obtained, which correspond to 72 cal cm^{-2} day^{-1} of latent heat. The energy balance shows 83 cal cm^{-2} to be available per day so that 11 cal cm^{-2} may be consumed for evaporation, giving rates of 0.2 mm day^{-1}. Evaporation thus only contributes about 2% to the total ablation. While these considerations are obviously simplified, the results are similar to the results by a number of authors investigating evaporation/melting ratios in polar regions: Ambach (1963), 1–5%, Greenland; Untersteiner (1961), 2%, Drifting Station A; Wendler (1967), 6%, Fairbanks.

The above considerations so far apply to the melting of a uniform snow cover. In reality, snow melts in a very irregular fashion, since its depth and density as well as exposure to radiation on a microscale varies appreciably. Fig. 3 shows the patchy mosaic of snow, water and exposed tundra surface in the last phases of snow melting. The immediate post-melting period gives daily latent heat fluxes of evaporation of 277 cal cm^{-2}, or evaporation rates of 4.6 mm day^{-1}, compared with 0.2 mm day^{-1} during melting. This is shown in Fig. 7 which also gives evaporation rates for all other periods, as well as factors that may affect the evaporation. Clearly, the considerably lowered albedo of patches of tundra that are snow-free allows absorption of more radiation and increases in air temperature. One may compare the energy characteristics of a snow-free patch with that of a melting snow surface by comparing heat balances for periods 3 and 2, respectively. Advection of available heat from bare tundra to snow patches will undoubtedly accelerate the ablation of the remaining snow. Assuming the tundra to consist of 50% melting snow and 50% bare tundra, and taking the mean of the heat balances for periods 2 and 3, the following picture emerges: the energy balance of the combined system is now $N=260$, $S=-32$, $Q=-48$, $E=-180$ cal cm^{-2} day^{-1}. Melting over half of the surface required $83/2=41$ cal cm^{-2} day^{-1}, leaving 139 cal cm^{-2} day^{-1} for evaporation. Evaporation over half of the tundra (the bare half) required $277/2=138$ cal cm^{-2} day^{-1}, leaving 1 cal cm^{-2} day^{-1} for evaporation from the snow. This is a lower limit; the upper limit is $139/2=70$ cal cm^{-2} day^{-1}, assuming both snow-free patches and snow surfaces to evaporate equally. Evaporation thus contributes between 1–13% to the ablation of snow patches, based on the above approximations.

In the last phases of melting, when small fragments of snow remain on the tundra, melting-to-evaporation ratios may change somewhat from the above results, depending on the size, shape and exposure to wind and radiation of the fragments as indicated by the computations of Hofmann (1963). Two of the factors limiting high evaporation rates are the amount of energy available and the much higher latent heats required for evaporation (600 cal gm^{-1}) compared with melting (80 cal gm^{-1}). Evaporation thus appears to play a minor role in the ablation of the snow cover. With increasing air temperature to well above freezing, the water vapor pressure will often rise above 6.1 mb, which is the saturation vapor pressure of melting snow. In other words, condensation rather than evaporation will then take place at the snow surface thereby increasing the rate of melting. For instance, during the snow melting period 4–13 June, the average daily water vapor pressure was at or above 6.1 mb for 5 of the 10 days, as determined from humidity measurements at the climatological weather station at Barrow.

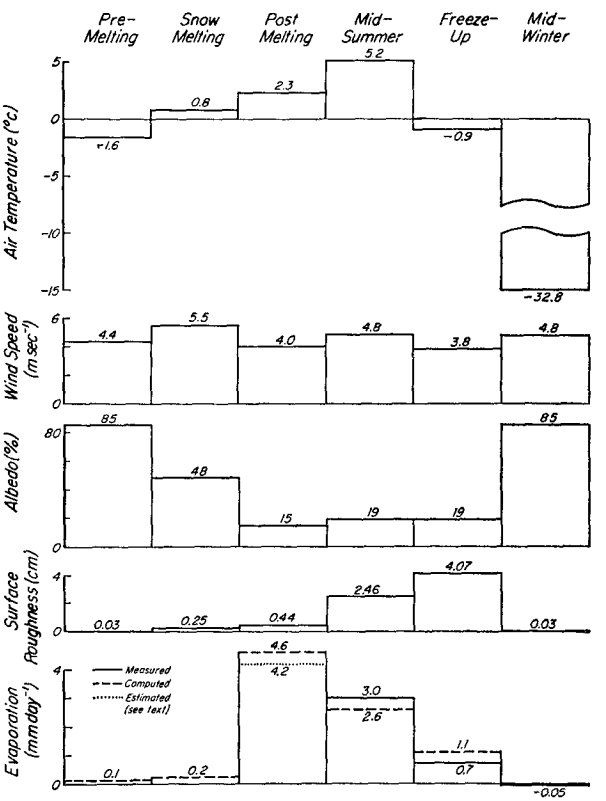

FIG. 7. Evaporation rates and factors that affect it, for the six identified characteristic periods.

This indicates that considerations of the heat budget alone cannot be used for estimating the rates of evaporation and further underlines that evaporation appears to play a minor role in the ablation of the snow cover in the Barrow area.

On the other hand, in areas of the Arctic Slope[1] where the snow cover is markedly thinner, and where the albedo is noticeably influenced by the dark snow-soil interface, grass or other type of vegetation penetrating through the snow, the ablation conditions may be quite different. According to measurements of solar radiation at Barrow (Maykut and Church, 1973), the average insolation in April and May approximately equals the insolation in June and July, due to higher albedos and multiple reflection in April and May and higher cloudiness in June and July. During April and the first half of May the air temperatures are essentially below freezing on the Arctic Slope, and it may be strongly suspected that evaporation can be a major factor in the ablation process, where the albedo is sufficiently low. In fact, ERTS images over the Brooks Range and the Arctic Slope during April–May, 1973 (Holmgren *et al.*, 1973), clearly show regression of snow over wide expanses on the foothills of the Brooks Range in April and early May, well before the air

[1] The area between the Brooks Range and the Arctic Ocean.

temperatures rise above freezing point. In this discussion, reference should be made to Benson (1969) who stressed the importance of evaporation and made detailed observations especially of the interaction between snow cover and the underlying vegetation.

The moisture regime for the summer as shown in Fig. 7, based on computed values from the energy balance, can be checked against actual evaporation measurements. These were carried out daily with a standard Class A evaporation tank. The tundra remains more or less wet throughout the summer and there is quite good agreement between measured and computed values as shown in Fig. 7. No measurements were available on the same days of period 3 for which balance computations are available. The estimated value of 4.2 mm day^{-1} is based on measured evaporation immediately following this period and probably underestimates the proper value. During period 5 ice had formed on the tank and unlike the tundra surface, did not melt diurnally. Measured evaporation values are thus also probably underestimates.

By winter, small pans were used to measure sublimation rates. Under conditions when no drift snow was blowing over the tundra, mean deposit rates of 0.05 mm ice per day were observed, corresponding to latent heat fluxes of 3 cal cm^{-2} day^{-1}. Deposition rates on elevated structures, such as the micrometeorological tower, were probably higher, since the wind and also transfer coefficients near these structures should be higher than at the flat tundra surface.

Climatic and terrain parameters, such as albedo and surface roughness, are also shown in Fig. 7 to allow comparisons. The wind regime can be seen to be fairly constant through the year; on the other hand, the strong decrease in albedo when the snow melts and absorbed solar radiation increases is the main factor in determining the evaporation off the tundra.

Acknowledgments. The authors thank Stan Parker, Dennis Trabant, Vaughn Rockney and Richard Schwartz for their active participation in the field work. This research was supported by the National Science Foundation under Grant GV-29342 to the University of Alaska. It was performed under the joint NSF sponsorship of the International Biological Program and the Office of Polar Programs and was directed under the auspices of the U. S. Tundra Biome. Field and laboratory activities at Barrow were supported by the Naval Arctic Research Laboratory of the Office of Naval Research.

REFERENCES

Ambach, W., 1963: Untersuchungen zum Energieumsatz in der Ablationzone des Gronlandischen Inlandeises. *Medd. Grønland,* **174**, No. 4, 311 pp.

Benson, C. S., 1969: The seasonal snow cover of Arctic Alaska. Res. Paper No. 51, Arctic Institute of North America, 86 pp.

Brown, J., and E. West, 1970: Tundra biome research in Alaska. The structure and function of cold-dominated ecosystems. U. S. IBP-Tundra Biome Rept. 70-1.

Hofmann, G., 1963: Zum Abbau der Schneedecke. *Archiv Meteor., Geophys. Bioklim.,* **B1**, 1–20.

Holmgren, B., C. B. Benson, and G. Weller, 1973: Survey of the seasonal snow cover of Alaska. Rept. No. 6, NASA-ERTS Contract NAS 5-21833, University of Alaska.

Jayaweera, K.O.L.F., and G. Weller, 1972: Physical properties of arctic stratus clouds. Paper presented at 53rd AGU meeting, Washington, D. C.

Lettau, H., 1949: Isotropic and non-isotropic turbulence in the atmospheric surface layer. Geophys. Res. Papers, No. 1, AFCRL, 86 pp.

Liljeqvist, G. H., 1956: Part 1: Energy exchange of an antarctic snow field. Short-wave radiation. *Norwegian-British-Swedish Antarctic Expedition, 1949–52, Scientific Results,* Vol. II, Norsk Polar Institutt, Oslo, p. 68.

Maykut, G. A., and P. E. Church, 1973: Radiation climate of Barrow, Alaska, 1962–66. *J. Appl. Meteor.,* **12**, 620–628.

Nakano, Y., and J. Brown, 1972: Mathematical modeling and validation of the thermal regimes in tundra soils, Barrow, Alaska. *Arctic Alpine Res.,* **4**, 19–32.

O'Neill, A. D. J., and D. M. Gray, 1972: Spatial and temporal variations of the albedo of prairie snow pack. International Symposium on the Role of Snow and Ice in Hydrology, Symposium on Properties and Processes, Banff., UNESCO-WMO-IASH, 176–186.

Trabant, D., C. Benson, and G. Weller, 1969: Physical-thermal processes in the seasonal snow cover of northern Alaska. *Proc. 20th Alaska Science Conf.,* University of Alaska, 328–332.

Untersteiner, N., 1961: On the mass and heat budget of arctic sea ice. *Arch. Meteor. Geophys. Bioklim.,* **A12**, 151–182.

Weller, G. and P. Schwerdtfeger, 1970: Thermal properties and heat transfer processes of the snow of the central antarctic plateau. IASH Publ. No. 86, *Proc. ISAGE Symp.,* Hanover, N. H., 284–297.

——, S. Cubley, S. Parker, D. Trabant, and C. Benson, 1972: The tundra microclimate during snow-melt at Barrow, Alaska. *Arctic,* **25**, No. 4, 291–300.

Wendler, G., 1967: The heat balance of the snow surface during the melting period (March, April 1966) near Fairbanks, Alaska. *Beitr. Geophys.,* **76**, 453–460.